Ocean heat transport in Simple Ocean Data Assimilation: Structure and mechanisms

Yangxing Zheng[1] and Benjamin S. Giese[2]

[1] The trend and variability of global ocean heat transport for the period 1958–2004 are investigated using the Simple Ocean Data Assimilation (SODA) analysis. The ocean model is forced with the European Center for Medium Range Weather Forecast (ECMWF) ERA-40 atmospheric reanalysis winds from 1958 to 2001 and with QuikSCAT winds from 2002 to 2004. The assimilation is based on a sequential estimation algorithm, with observations from the historical archive of hydrographic profiles supplemented by ship intake measurements, moored hydrographic observations and remotely sensed sea surface temperature. Heat transport is calculated using temperature and velocity from the ocean analysis. Mean heat transport from the analysis generally agrees with previously published estimates from observational and modeling studies. Trends of heat transport show a range of behaviors. In the Atlantic and Pacific Oceans there is mostly increasing poleward heat transport with two important exceptions. In the Atlantic Ocean there is decreasing heat transport around 50°N and 60°N, and in both the Atlantic and Pacific Oceans there is decreasing heat transport near 10°S. There is also prominent interannual and decadal variability in all of the ocean basins. The results suggest that ocean heat transport variability is primarily determined by the strength of the meridional overturning circulation (MOC), which is controlled by complex processes governing fresh water flux in the northern North Atlantic and surface wind stress. However, the role of temperature variability increases at high latitude, particularly in the northern North Atlantic Ocean. Eddies play an important role in heat transport in the Gulf Stream and its extension in the Atlantic Ocean, and the Kuroshio and its extension in the Pacific Ocean and enhanced Subtropical cells (STCs) affect heat transport estimates in the tropics. In the northern North Atlantic Ocean, a small increase in meridional heat transport and a slight weakening of MOC are detected. Weakening in the northern North Atlantic MOC mainly arises from a freshening in the Labrador Sea and slowdown of the overflows from the Nordic Seas into the northern North Atlantic Ocean. Trends in North Atlantic surface momentum forcing are uniform across several atmospheric reanalyses, however there is less agreement in the role of precipitation in forcing trends of MOC and this exists as a primary source of uncertainty in our analysis.

Citation: Zheng, Y., and B. S. Giese (2009), Ocean heat transport in Simple Ocean Data Assimilation: Structure and mechanisms, *J. Geophys. Res.*, *114*, C11009, doi:10.1029/2008JC005190.

1. Introduction

[2] Understanding variability of heat transport (or more properly enthalpy [*Warren*, 1999]) by the Oceans is critically important to understanding climate and climate change. Early studies of ocean heat transport [e.g., *Sverdrup et al.*, 1942; *Vonder Haar and Oort*, 1973; *Hastenrath*, 1980, 1982; *Newell and Chiu*, 1981; *Talley*, 1984; *Carissimo et al.*, 1985; *Hsiung*, 1985; *Trenberth and Solomon*, 1994]

found that the ocean contribution to heat transport is comparable to that of the atmosphere. In contrast, *Trenberth and Caron* [2001] calculate ocean heat transport (OHT) as the difference between directly calculated atmospheric heat transport and satellite measurements of net radiation at the top of the atmosphere and find that the overall Northern Hemisphere atmospheric heat transport is larger than ocean transport, with poleward ocean heat transport dominant only between 0° and 17°N. Using in situ oceanic measurements *Wunsch* [2005] shows that the Northern Hemisphere Oceans and atmosphere carry comparable poleward heat fluxes to about 28°N at which latitude the oceanic poleward flux decreases as heat is lost to the atmosphere. These results are qualitatively similar to those of *Trenberth and Caron* [2001], with the major exception that the gradual reduction in oceanic heat transport is at high northern latitudes. *Fasullo*

---

[1]Climate Diagnostics Center, Physical Sciences Division, ESRL, CIRES, NOAA, Boulder, Colorado, USA.

[2]Department of Oceanography, Texas A&M University, College Station, Texas, USA.

and Trenberth [2008a, 2008b] and *Trenberth and Fasullo* [2008] compute ocean energy divergence as a residual of the atmospheric energy budget, which address energy transport in the atmosphere and Oceans. These studies use top of atmosphere (TOA) net radiation from the Earth Radiation Budget Experiment (ERBE) and Clouds and the Earth Radiant Energy System (CERES) satellite observations and the complete atmospheric energy budget tendency and divergence. They show that although estimates of the annual and zonal mean meridional ocean energy transport does not differ greatly from previous studies, there are important differences in the North Atlantic. They also show that the strongest poleward energy transport in each hemisphere occurs during the cold season.

[3] Heat transport in individual ocean basins can be difficult to directly estimate due to a scarcity of ocean measurements. As more hydrographic data sets became available during the World Ocean Circulation Experiment (WOCE), direct estimate of individual ocean basin heat transport became possible, particularly in the Atlantic Ocean. For example, *Ganachaud and Wunsch* [2003] use hydrographic sections in combination with a geostrophic inverse model to provide a mean value of global and individual ocean heat transport with self-consistent error bars. Their uncertainties of estimated heat transport include those for Ekman transport, which are 50% of the initial value and model error, which is dominated by aliasing of oceanic variability by synoptic scale variability as sections are sampled in different years and seasons.

[4] The transport of heat from individual oceanic observations show that throughout the Atlantic Ocean and in the North Pacific heat transport is northward [*Bryan*, 1962; *Bennett*, 1978; *Hall and Bryden*, 1982; *Roemmich and Wunsch*, 1985; *Rago and Rossby*, 1987; *Molinari et al.*, 1990; *Rintoul*, 1991; *Friedrichs and Hall*, 1993; *Wijffels et al.*, 1996; *Fillenbaum et al.*, 1997; *Robbins and Toole*, 1997; *Lavin et al.*, 1998; *Macdonald*, 1998; *Koltermann et al.*, 1999; *Ganachaud and Wunsch*, 2000, 2003; *Talley*, 2003]. It is more difficult to determine the dominant direction of meridional heat transport in the South Pacific because of a lack of measurements there. *Trenberth and Caron* [2001] suggest a southward annual mean heat transport based on the surface fluxes for February 1985 to April 1989. The dominant direction of heat transport in the Indian Ocean is predominantly southward, a result that is consistent in many previous studies [e.g., *Robbins and Toole*, 1997; *Macdonald*, 1998; *Ganachaud and Wunsch*, 2000; *Sloyan and Rintoul*, 2001a; *Talley*, 2003]. Since observations of the Atlantic Ocean are more abundant than in the other two ocean basins, heat transports across specified sections can be used to estimate heat transport variability. These estimates, made with different data sets, and with different computation methods, suggest that there is large variability of ocean heat transport on a wide range of time scales. As noted by *Trenberth and Caron* [2001], there are two major disadvantages of estimating ocean heat transport using ocean observations. One is that estimates can only be made at a few locations for which high quality observations are available and that several assumptions, such as using geostrophic velocity estimates, are usually employed. Another substantial disadvantage of using direct

ocean observations to estimate heat transport is inadequate temporal sampling and resolution of the annual cycle.

[5] In this paper we use the results of an ocean analysis that covers the period from 1958 to 2004 to describe the change in enthalpy and heat transport of the global Oceans. Use of the analysis allows us to calculate heat transport using the model currents and temperatures which are constrained by observations.

2. Simple Ocean Data Assimilation Analysis

[6] The multiyear Simple Ocean Data Assimilation (SODA) analysis is used to explore the variability of oceanic heat transport and to identify the processes responsible for the characteristics of heat transport in the world's Oceans. The SODA methodology, the ingested data, and the error covariance structure of both the model and the observations are described by *Carton et al.* [2000] and *Carton and Giese* [2008]. Briefly, The ocean model is based on the Los Alamos implementation of the Parallel Ocean Program (POP) [*Smith et al.*, 1992]. The model resolution is an average $0.4°$ (longitude) X $0.25°$ (latitude) with 40 vertical levels. The model is forced with the European Center for Medium-Range Weather Forecasts (ECMWF) ERA-40 atmospheric reanalysis winds [*Simmons and Gibson*, 2002] for the 44 year period from 1958 to 2001. The analysis is continued from 2002 to 2004 using QuikSCAT wind stress.

[7] Surface heat fluxes are computed using bulk formulae, with atmospheric variables that come from the NCAR/NCEP reanalysis. The NCEP/NCAR reanalysis information is used for the bulk formula instead of the ERA-40 variables throughout the experiment to give continuity of surface forcing during periods for which the ERA-40 winds are not available. Surface freshwater flux is provided by the Global Precipitation Climatology Project (GPCP) monthly satellite gauge merged product [*Adler et al.*, 2003] combined with evaporation obtained from a bulk formula. For the period before 1979, a climatology based on GPCP is used. Vertical diffusion of momentum, heat, and salt is based on a nonlocal KPP scheme and horizontal diffusion for subgrid-scale processes is based on a biharmonic mixing scheme.

[8] The model is constrained by observed temperature and salinity using a sequential assimilation algorithm which is described by *Carton et al.* [2000] and *Carton and Giese* [2008]. The basic subsurface temperature and salinity data sets consist of approximately 7×10^6 profiles, of which two thirds have been obtained from the World Ocean Database (WOD) 2001 [*Boyer et al.*, 2002; *Stephens et al.*, 2002]. This data set is extended by operational temperature profile observations from the National Oceanographic Data Center/ NOAA temperature archive, including observations from the TAO/Triton mooring thermistor array and Argo drifters. In situ and satellite sea surface temperature is also used in the data assimilation processes.

[9] Some recent studies suggest that the drop rates assumed for XBTs likely are contaminated by drop rate bias [*Ivchenko et al.*, 2006; *Willis et al.*, 2007; *Gouretski and Koltermann*, 2007]. These instruments suffered from biases in drop rates and much effort since then has been devoted to correcting for these biases. The version of SODA

that we use (SODA 1.4.2/1.4.3) use the drop rate correction described by *Stephens et al.* [2002].

[10] Model output, such as temperature, salinity, and velocity are averaged over 5 day intervals. These average fields are then mapped onto a uniform global 0.5° (longitude) X 0.5° (latitude) grid using the horizontal grid Spherical Coordinate Remapping and Interpolation Package with second order conservative remapping [*Jones*, 1999]. Some modest smoothing results from the remapping, however the method conserves the mass transport, which is important in the calculation of heat transport. The mapping shifts the locations of the temperature and horizontal velocity grids, which are offset in the model, to the same set of remapped grid point locations.

3. Results

3.1. Heat Transport Mean and Trend

[11] We begin by describing the mean heat transport of the global Oceans, given by the integral $C_p \int_{-D}^{0} dz \int_{west}^{east} \rho V (T - T_r)\, dx$, where C_p is the seawater heat capacity under constant pressure, D is the depth of ocean, ρ is the in situ ocean water density, V is current velocity and $T - T_r$ is temperature minus a reference temperature which we take to be 0°C. We follow the oceanographic literature and refer to this integrated quantity as heat transport (see *Warren* [1999] for an expanded discussion of heat transport and enthalpy). Of course heat transport defined in this way cannot account for recirculation, since there can be a net flow through a section. But there is no obvious way to insure that there is no net flow through a section, and so we use the actual model velocity. It is the divergence of ocean heat transport (i.e., heat flux) that has a physical impact on the atmosphere. Therefore, even with a net transport, the divergence of heat transport between two latitudes is well defined.

[12] Figure 1a shows the long-term mean and standard deviation (in parentheses) of ocean heat transport in PW (1 PW = 10^{15} W) across sections for the period 1958–2004 using SODA data. Since the purpose of this study is to investigate the variability of ocean heat transport on time scales greater than one year, the standard deviation is calculated after the removal of the annual cycle. Northward mean heat transport in the Atlantic Ocean is reasonably consistent with results from many previous studies [*Bryan*, 1962; *Bennett*, 1978; *Hall and Bryden*, 1982; *Roemmich and Wunsch*, 1985; *Rago and Rossby*, 1987; *Molinari et al.*, 1990; *Rintoul*, 1991; *Friedrichs and Hall*, 1993; *Wijffels et al.*, 1996; *Fillenbaum et al.*, 1997; *Robbins and Toole*, 1997; *Lavin et al.*, 1998; *Macdonald*, 1998; *Koltermann et al.*, 1999; *Ganachaud and Wunsch*, 2000, 2003; *Holfort and Siedler*, 2001; *Talley*, 2003], with estimated heat transport values that range from 0.38 to 1.09 PW and with maximum heat transport in the midlatitudes. Further north, heat transport falls off rapidly because of cooler temperatures. The dominant northward ocean heat transport throughout the Atlantic Ocean is primarily associated with the thermohaline circulation in which North Atlantic Deep Water is formed in the polar and subpolar North Atlantic and subsequently flows southward throughout the Atlantic. In the Pacific Ocean, northward heat transport also dominates, although its magnitude is much smaller than that at the same latitude

in the Atlantic Ocean. The northward heat transport in the North Pacific is mainly due to a shallow Ekman upper thermocline cell [*Wijffels et al.*, 1996]. In the Pacific Ocean, the peak heat transport occurs in a narrow band centered on 20°N. It is not surprising to find that heat transport in the South Pacific is also northward. This is due to the fact that warm water in the Pacific is transported to the Indian Ocean via the Indonesian Throughflow (about 1.22 ± 0.13 PW is transported), giving rise to a large southward heat transport in the Indian Ocean [*Ganachaud and Wunsch*, 2000] and forcing flow northward in the South Pacific Ocean. Heat transport is found to have strong variability at lower latitudes and weak variability at middle and high latitudes in the world Oceans. Particularly, the strongest variability of heat transport is in the tropical Pacific Ocean and reflects the considerable impact of El Niño-Southern Oscillation (ENSO). In the Southern Ocean zonal heat transport has relatively weak variability. The large zonal heat transport of 2.2 PW south of Australia is due to the large contribution of about 1.3 PW of southward heat transport from the Indian Ocean, and so these transports represent heat circulating around Australia.

[13] Figure 1b portrays the trend in PW decade^{-1} of ocean heat transport. Most of the Atlantic Ocean has increasing poleward heat transports, with two important exceptions. At high latitudes (around 50°N and 60°N) and at 10°S there is a tendency toward weakening northward heat transport. The trends in the North Atlantic Ocean south of 40°N are considerable. For example, the trend of 0.054 PW decade^{-1} at 30°N in the Atlantic Ocean implies a 0.26 PW increase of heat transport from 1958 to 2004, which is much larger than its uncertainty of 0.15 PW. Although heat transport trends are not significant at the 95% confidence level at 10°S, 50°N, and 60°N, the negative trends may provide some useful information about the change of the Atlantic meridional overturning circulation (MOC). Heat transport trends in the Pacific are also not small (although they are mostly not significant at the 95% confidence level), but there is far less uniformity in the sign of the transport. The tropical and South Pacific mostly has an increasing trend of northward heat transport, but as with the Atlantic Ocean, at 10°S there is a decreasing heat transport. The trends in the Indian Ocean are much smaller than in the Atlantic Ocean, and are not of a uniform sign. Heat transport from the Pacific Ocean to the Indian Ocean via the ITF has a decreasing trend. Since in this study we focus on the heat transport in the Atlantic Ocean, we further examine the linear trend of heat transport in the Atlantic Ocean by plotting their time series, shown in Figure 2, along with R^2 which represents "explained variance" of the fitted line (the dashed line in Figure 2).

3.2. Characteristics of Heat Transport Variability

[14] There are two major mechanisms that can affect the variability of ocean heat transport. One is that the mean currents can advect anomalous temperature ($\overline{V}\, T'$) and another whereby anomalous currents advect the mean temperature ($V'\, \overline{T}$). Here a primed quantity represents its departure from its (monthly) climatology and a bar represents the monthly climatology. *Seager et al.* [2001] posit that changes in the oceanic meridional heat transport in the tropical Atlantic Ocean are dominated by $\overline{V}\, T'$. In contrast, *Schott et al.* [2004] provide evidence that within the wind-
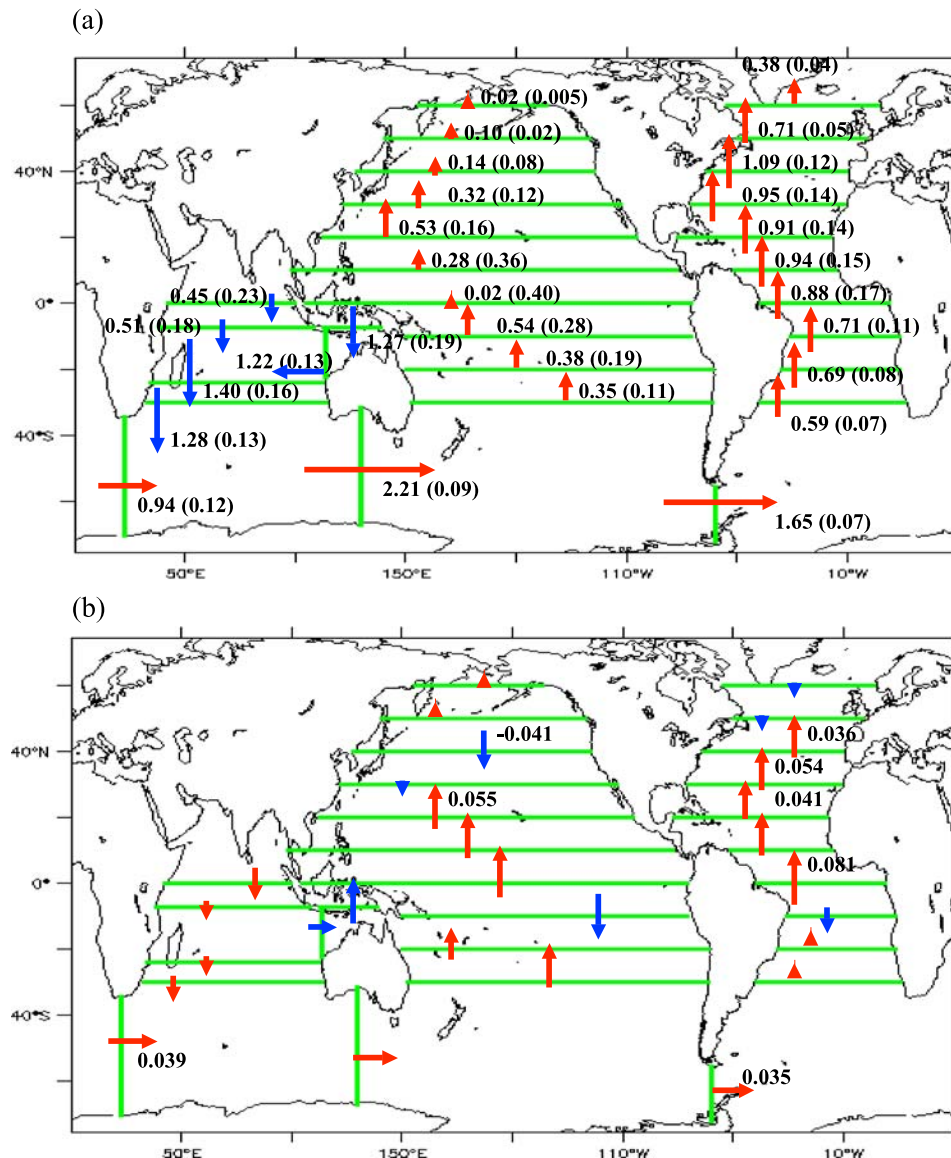
(a)

(b)

Figure 1. (a) Long-term mean and standard deviation (in parentheses) of oceanic heat transport in PW (1 PW = 10^{15} W) across sections and (b) trend of oceanic heat transport in PW decade^{-1} for the period 1958–2004. Only values that exceed a significance of 95% are shown.

driven Subtropical Cells (STC) the $V' \bar{T}$ process is more important than advection of subducted temperature anomalies by the mean STC currents in forming equatorial SST anomalies.

[15] SODA can be used to determine which of these two mechanisms is responsible for variability of ocean heat transport. Observational and modeling studies show interannual to decadal variability of ocean heat transport in the Atlantic Ocean can be linked to the MOC and horizontal gyre circulation. For example, *Bryden et al.* [2005] describe a slowing of the Atlantic Ocean's MOC at 26°N which they argue caused a decrease of the northward heat transport by 30% over the past 50 years. Although this weakening MOC is debated, it is an important issue. Because there is heat exchange between the ocean and the atmosphere, a disruption or collapse of MOC is likely to impact the global climate. The role of horizontal ocean gyre circulation variability in heat transport variability is still not well

addressed, even in the Atlantic and Pacific Oceans. The Gulf Stream and deep western boundary currents (DWBC), important components of horizontal circulation, combine to play an important role in ocean heat transport, since warm water is transported northward by the Gulf Stream in the upper layer and cold water is transported equatorward by the DWBC at depth, thus linking the MOC and gyre circulations. However, on a basin-wide scale, vertically integrated ocean circulation on horizontal plane (i.e., gyre circulation) could be argued to be a less relevant diagnostic than the zonally integrated ocean circulation on meridional plane (i.e., MOC) in generating mean meridional oceanic heat transport because the horizontal temperature difference between poleward warm water transport and equatorward cold water transport is generally much smaller than the vertical temperature difference between the warm surface water transported poleward and cold water that returns at depth.
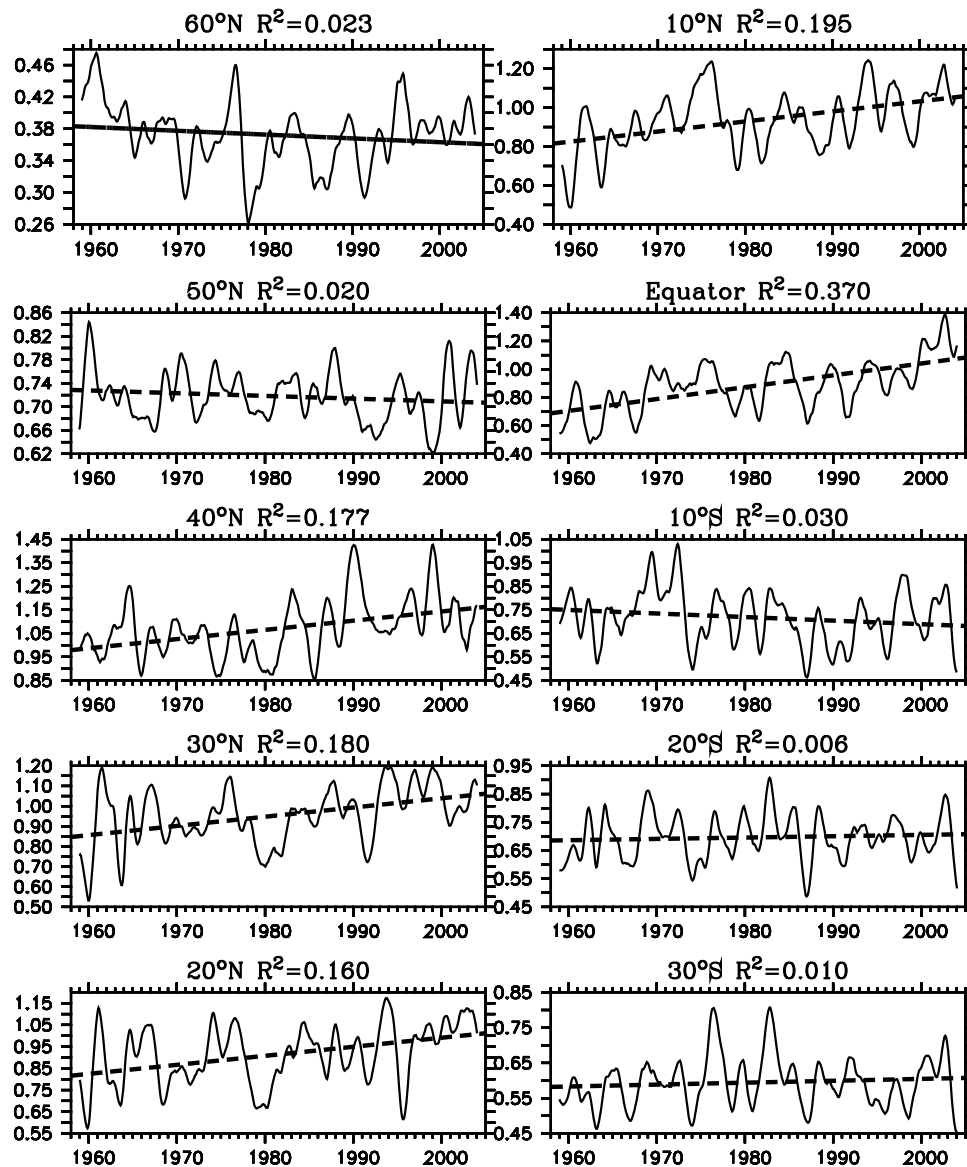
Figure 2. Time series of heat transport in PW and their linear trends in the Atlantic Ocean with R^2 denoted. Trends are significant at a 95% confidence level at the Equator, 20°N, 30°N, and 40°N.

[16] Interannual to decadal variability of meridional ocean heat transport for the Atlantic, Pacific and Indian Oceans is shown in Figure 3. Heat transport variability has a lot in common among the three ocean basins. First, variability of oceanic heat transport for the three ocean basins is highly dependent on latitude. At low latitudes, interannual variability dominates, whereas at middle and high latitudes, decadal or multidecadal variability is more pronounced. The interannual variability of oceanic heat transport at low latitudes is much stronger than the decadal variability at high latitudes. For instance, ocean heat transport variability ranges from −0.6 PW to +0.6 PW in the tropical Atlantic, whereas decadal variability varies from −0.2 PW to +0.2 PW in the North Atlantic. Similar behavior is found in the Pacific and Indian Oceans. Results from spectral analysis (not shown) also show a latitudinal dependence of timescales of variability in ocean heat transport.

[17] It is also evident that there are differences of interannual to decadal variability between the three ocean basins. The regions of robust interannual variability extend to 40°N in the Atlantic Ocean, while in the Pacific Ocean strong interannual variability of ocean heat transport is confined to the region between 10°S and 10°N. This behavior in the Pacific is likely related to the strong ENSO signal, and indeed there is much stronger interannual variability of ocean heat transport in the equatorial Pacific than in the equatorial Atlantic. The low frequency variability of heat transport in the Indian Ocean is mostly near or south of the equator (30°S–10°N).

3.3. Mechanisms of Variability of Ocean Heat Transport

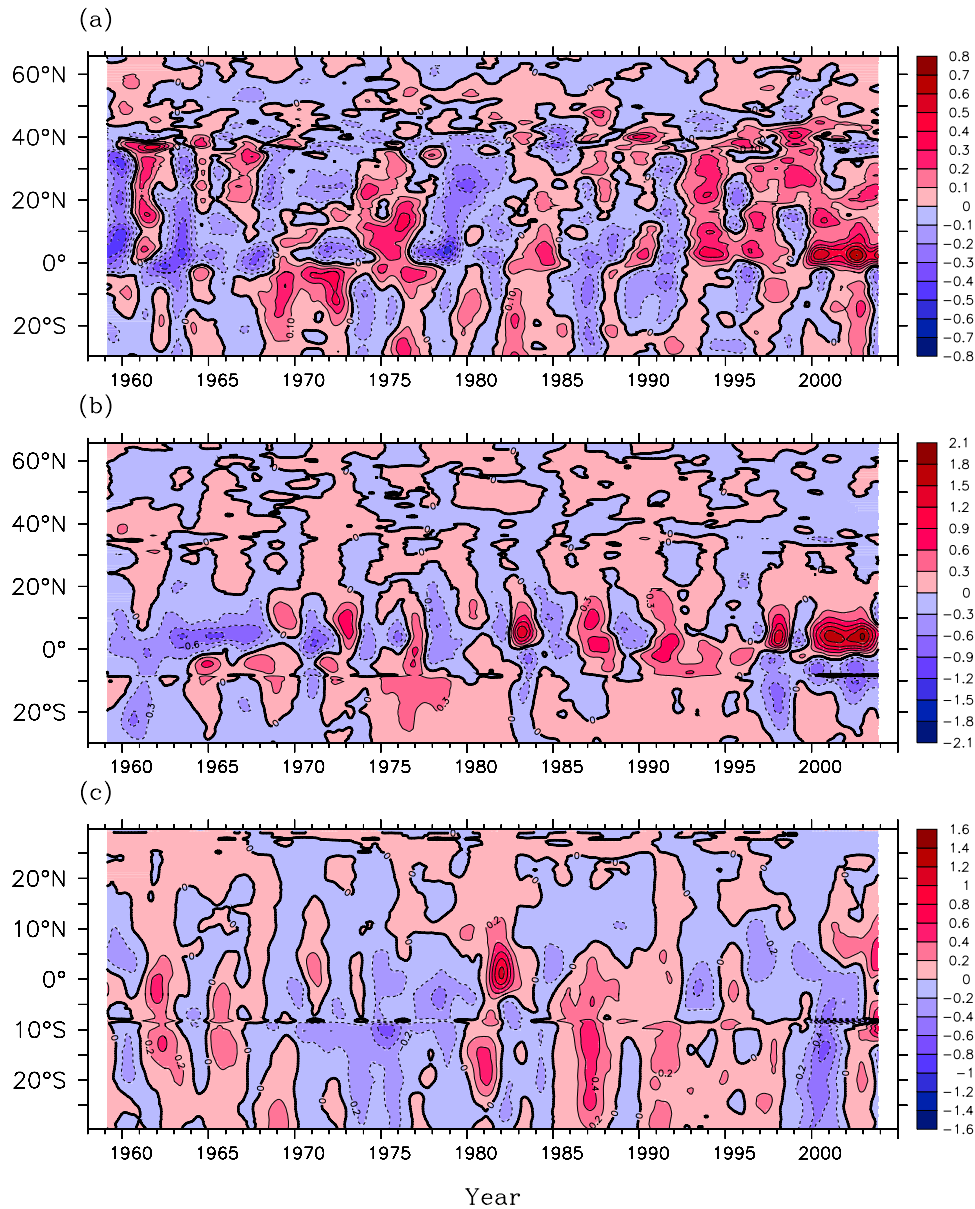[18] To explore the mechanisms responsible for heat transport variability, it is useful to decompose the heat

Figure 3. Latitude-time evolution of meridional heat transport anomalies in PW in the (a) Atlantic, (b) Pacific, and (c) Indian Oceans derived from the analysis over the period 1958–2004. Red (blue) shading indicates positive (negative) anomalies.

transport equation. Anomalies of heat transport are generated by three terms

$$VT = \left(\overline{V} + V'\right)\left(\overline{T} + T'\right) = \overline{V}\,\overline{T} + V'\overline{T} + \overline{V}T' + V'T', \quad (1)$$

with only the last three terms on right hand side in equation (1) contributing to interannual or decadal variability of ocean heat transport.

[19] Anomalies of total meridional heat transport in PW at 30°N in the Atlantic Ocean, chosen as being representative of a midocean basin, are shown in Figure 4 together with its three contributing components. The term $V'\,\overline{T}$ clearly contributes most to anomalies of total meridional heat transport. Next in importance is $\overline{V}\,T'$, while variations of $V'T'$ are small. This implies that variability of total heat

transport at 30°N Atlantic Ocean is predominantly induced by change in ocean currents. Temperature change, at least in this region, is not as important in generating variability of ocean heat transport.

[20] In order to examine whether changes in current velocity is a dominant factor in producing variability of ocean heat transport in the global Oceans, we evaluate the contributions from the three terms to total heat transport variability at several locations. We calculate the percentage of variance explained by each of the three terms from equation (1) in 10° bins in each of the ocean basins. The contribution in percentage from $V'\,\overline{T}$, $\overline{V}\,T'$, and $V'T'$ to the total meridional heat transport anomalies is shown in Figure 5 for the Atlantic, Pacific, and Indian Oceans. It is clear that the term $V'\,\overline{T}$ accounts for the greatest contribution to variability of the total meridional heat transport for
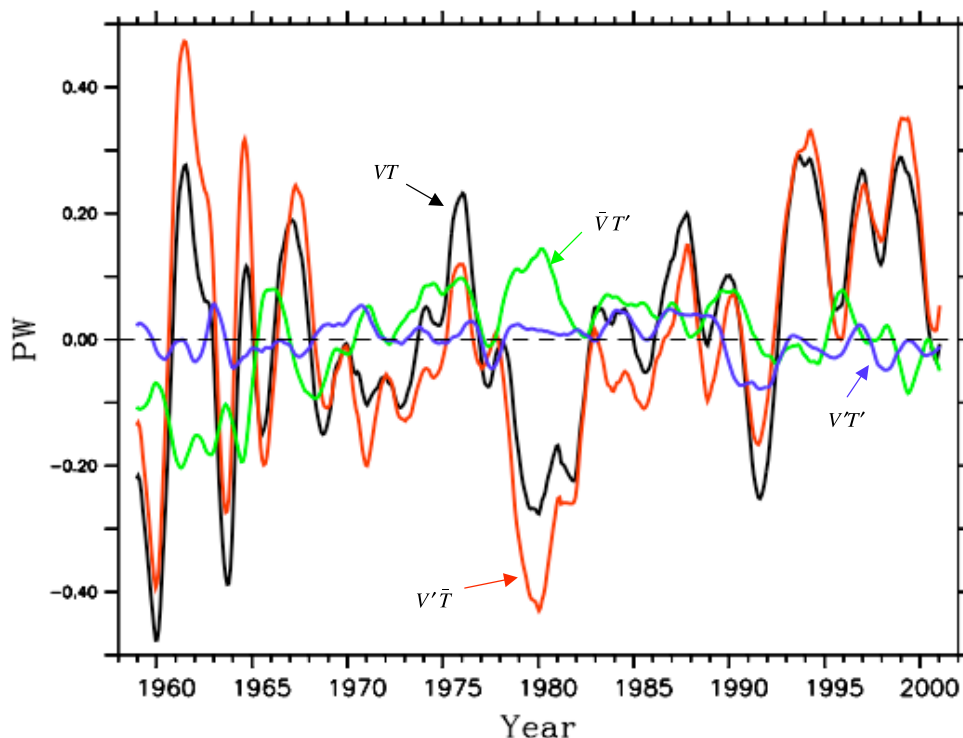
Figure 4. Anomalies of total meridional heat transport in PW at 30°N in the Atlantic Ocean (black). Three contributing components are shown: red shows the contribution from $V' \bar{T}$, green indicates the contribution from $\bar{V} T'$, and blue shows the contribution from $V' T'$.

most regions in all three basins. However, there are some notable exceptions. In the North Pacific and Atlantic Oceans $\bar{V} T'$ can be important. For example, at 60°N in the Atlantic $\bar{V} T'$ is more important than $V' \bar{T}$. The fact that contributions from $V'T'$ are large at 40°N in the Atlantic and Pacific Ocean shows that eddies become important in the regions of the Gulf Stream extension region in the Atlantic and the Kuroshio and Kuroshio extension region of the Pacific Ocean, even though eddies are not well resolved by the model resolution. Figure 5d shows zonal heat transport in the ITF region (115°E) and at the tree "choke points" between continents and the coast of Antarctica. Variability of zonal heat transport in the ITF (115°E) is also predominantly controlled by currents. In contrast with the ITF, heat transport in the Southern Ocean has an important contribution from $\bar{U} T'$ and is even the dominant term.

3.4. Climate Mechanisms for OHT

3.4.1. Strength of MOC and Gyre Circulation

[21] In order to determine how ocean heat transport responds to MOC and gyre circulation it is necessary to define the strength of MOC and the gyre circulation. It is usually difficult to quantify the strength of ocean circulation because of overlapping forcing mechanisms. For example, wind stress variability can contribute to changes both in MOC and the gyre circulation. In fact the circulations themselves overlap, making the definition of an index of circulation difficult. By confining attention to a limited domain, a unique index defined to depict the strength of the ocean circulation is possible. The conventional method for defining the strength of the basin-scale ocean circulation is to locate the maximum value of the stream function, and

then to use the maximum value as an index of ocean circulation.

[22] The mean gyre circulation and MOC in Sv (1 Sv = 10^6 m^3 s^{-1}) for the Atlantic, Indo-Pacific Oceans are shown in Figure 6 by contouring the horizontal and meridional overturning stream functions. The subtropical and subpolar gyres are clearly identified in the Atlantic and Pacific Oceans. The subtropical gyres in the Atlantic and Pacific Oceans have a maximum volume transport of more than 40 Sv. The vertical stream function in the Atlantic shows that wind-driven shallow overturning cells overlay the density-driven intermediate (500–2000 m) and deep overturning cells associated with deep water formation. The maximum stream function value at 36°N in the North Atlantic is about 20 Sv, half of the subtropical gyre circulation. The MOC in the Indo-Pacific is quite different from that of the Atlantic. The strongest meridional overturning cells in the Indo-Pacific Oceans are in the upper 400 m with a strength of more than 20 Sv. The deep cells in the Indo-Pacific Oceans are weak and irregular as compared to those of the Atlantic Ocean.

3.4.2. OHT Response to MOC and Gyre Circulation

[23] We choose 36°N as the location of both the maximum meridional overturning stream function and maximum horizontal stream function for the North Atlantic. The deep cell is weak in the Pacific and so the maximum overturning is at 14°N, whereas the maximum gyre circulation is at 35°N. An index derived from anomalies of these peak values is chosen to define the strength of anomalous ocean circulation and anomalies of meridional heat transport are linearly regressed onto the index. The meridional ocean heat transport response to the Atlantic MOC/gyre and Pacific
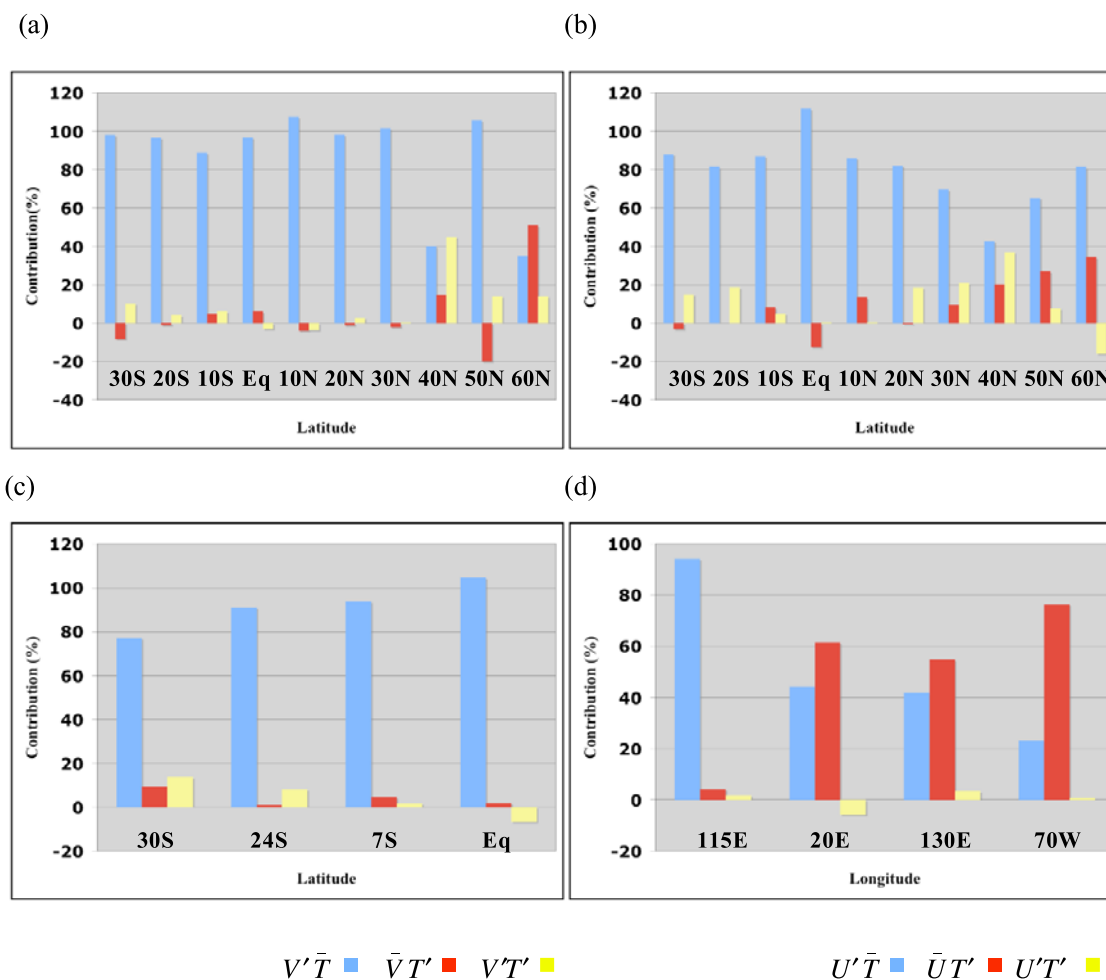
(a)　　　　　　　　　　　　　　　　　　(b)

(c)　　　　　　　　　　　　　　　　　　(d)

$V'\,\bar{T}$ ■　$\bar{V}\,T'$ ■　$V'T'$ ■　　　　　　$U'\,\bar{T}$ ■　$\bar{U}\,T'$ ■　$U'T'$ ■

Figure 5. Contributions in percentage of $V'\,\overline{T}$ (blue), $\overline{V}\,T'$ (red), and $V'\,T'$ (yellow) to total meridional heat transport anomalies VT in the (a) Atlantic, (b) Pacific, and (c) Indian Oceans and (d) contributions to zonal heat transports in the ITF and in the Southern Ocean.

STC/gyre is shown in Figure 7. Ocean heat transport regressed onto the meridional circulation index is much stronger than when regressed onto the gyre circulation index in both the Atlantic and Pacific Oceans. This implies that meridional heat transport in the Oceans is primarily governed by ocean circulation in the meridional-vertical plane instead of the horizontal plane. However, the spatial patterns of response in the Atlantic and Pacific are different. In the Atlantic there are two peak values of heat transport, one near the Equator and one near 30°N. In contrast, the Pacific transport has only one peak value, which is near 8°N. In the Atlantic the response to MOC appears to be within a latitudinal band from the Equator to 40°N, whereas in the Pacific the response is from 20°S to 20°N. This structure of response in latitudinal bands is probably linked to the spatial features of meridional heat transport as shown in Figure 3. Because the linear trend in the strength of the STC in the Pacific Ocean (-0.11 Sv decade^{-1}) is much smaller than its counterpart in the Atlantic Ocean (0.71 Sv decade^{-1}), we focus next on the Atlantic Ocean.

3.4.3. Evolution of the Atlantic MOC and Associated OHT

[24] Figure 8 shows the evolution of anomalous Atlantic MOC stream function and meridional heat transport for the period 1958 through 2004. At low to midlatitudes, anomalous meridional heat transport is synchronous with the strength of the Atlantic MOC on interannual to decadal timescales. At high latitude, this relationship is less pronounced. The difference of ocean heat transport in response to strength of MOC at low and high latitude reflects the relative importance of the roles of ocean currents and temperature fields in heat transport at different latitudes. These are illustrated in Figure 5 whereby in the region south of 50°N the change in currents dominates heat transport variability, and in regions poleward of 50°N the importance of temperature grows and so it is a mixture of variability in currents and temperature fields that describes the variability of heat transport.

[25] Linear changes in the strength of MOC and in ocean heat transport as a function of latitude are shown by a solid curve in Figure 8 which is red when the change exceeds the 95% significance level using a student t test. One standard deviation of MOC and ocean heat transport is denoted by a dashed curve. There is a significant change in heat transport at three latitudinal bands: 1°S−5°N, 18°N−22°N, and 39°N−44°N while change in MOC is not significant except in the northern North Atlantic Ocean (55°N−62°N). An interesting feature of the Atlantic MOC is that it tends to
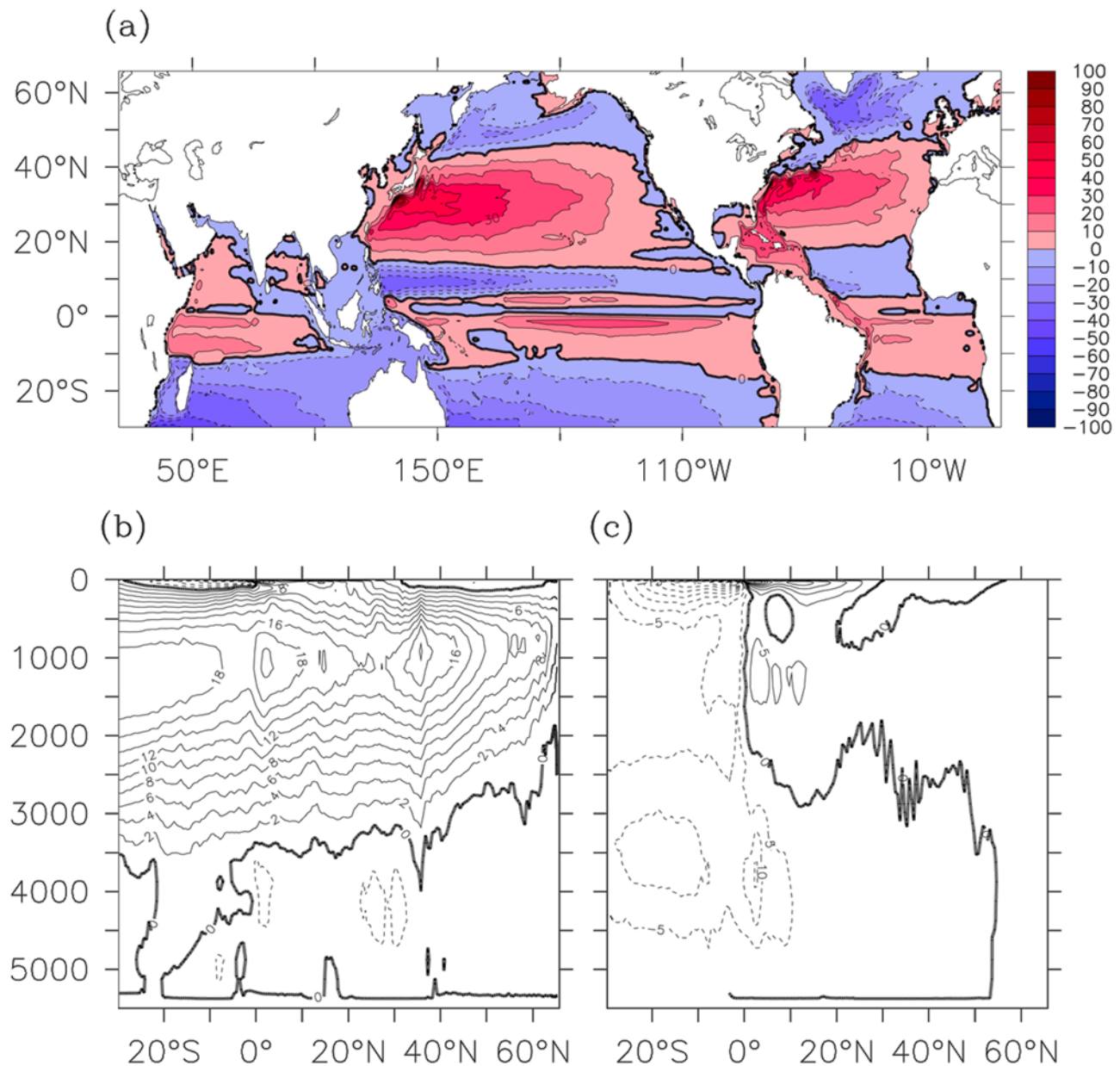
Figure 6. (a) Mean gyre circulations of the Atlantic and Indo-Pacific Oceans in terms of the mean horizontal stream function and (b and c) mean meridional overturning circulations of the Atlantic (Figure 6b) and Indo-Pacific (Figure 6c) Oceans depicted by the meridional overturning stream function. Unit for stream function is Sv (1 Sv = 10^6 m^3 s^{-1}).

weaken in the northern North Atlantic Ocean and tends to strengthen in the region south of 40°N. This bidirectional signal in the strength of the Atlantic MOC implies a convergence of water in the region between 40°N and 50°N. It also implies that change of MOC strength estimated at a few latitudes may not represent the change of the basin-scale MOC. Another intriguing feature of the relationship between ocean heat transport and MOC change is apparent at high latitude. Although the MOC tends to weaken in the northern North Atlantic Ocean, there is a slight increase in ocean heat transport at some high latitudes for the period 1958–2004. In the following section, we will explore the possible causes of the Atlantic MOC changes.

3.5. Possible Causes of Atlantic MOC Changes

3.5.1. Weakening in the Northern North Atlantic Ocean

[26] The spatial pattern of the linear changes for 47 years of τ_x, SST, ρ, and salinity in the region of the North Atlantic Ocean 40°N–70°N is shown in Figure 9. There are several interesting features in the change of surface density. First, a relatively large area of surface water in the Labrador Sea (between 48°N and 60°N, west of 50°W) becomes much lighter (~−0.2 kg m^{-3}), particularly in the sinking region. The decrease in surface density there can be expected to slow down the sinking process, hence may be an important factor in affecting the strength of the Atlantic MOC. An
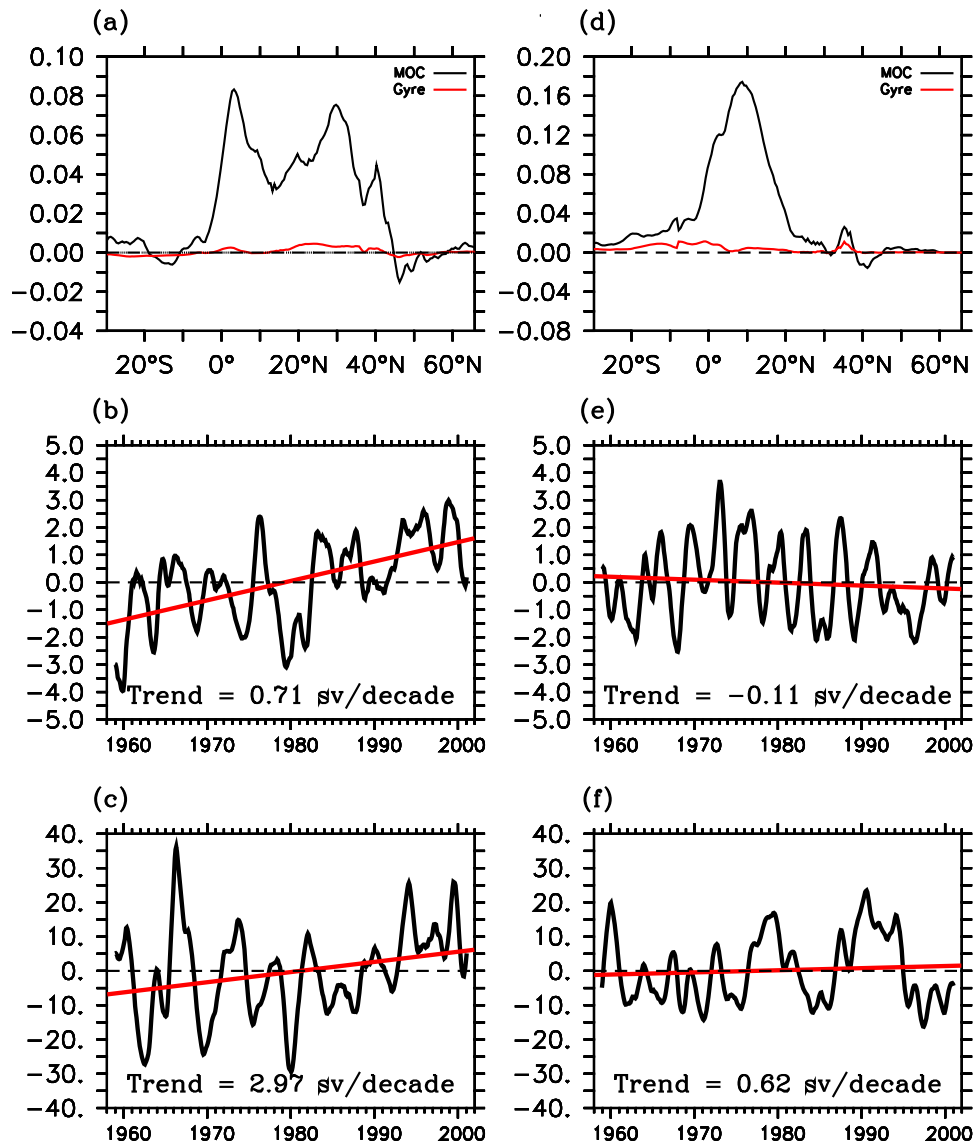
Figure 7. Meridional heat transport response to strength of MOC and gyre circulation in the (a) Atlantic and (d) Pacific Oceans (units are PW Sv^{-1}). Anomalies and trends of the Atlantic (b) MOC and (c) gyre and the Pacific (e) MOC and (f) gyre are also shown. Unit for anomaly of Atlantic MOC, Atlantic gyre, Pacific MOC, and Pacific gyre is Sv.

enhanced τ_x can lead to local cooling, thus generating denser water. But why does surface density decrease given that wind stress is strengthening? One explanation is that there is a decrease in salinity due to freshening that counteracts the cooling effect by strengthening wind stress. At high latitude in the North Atlantic Ocean, where water is cold, salinity rather than temperature, dominates the change of water density. Therefore a large discharge of fresh water into the high latitude region inhibits sinking, giving rise to a weaker MOC. Freshwater discharge in the North Atlantic Ocean is primarily from the Arctic Ocean via the Labrador and East Greenland Currents and adjacent river runoff and precipitation. Figure 9 suggests an important influence of salinity on the surface density, particularly in the Labrador Sea.

[27] Cold water overflow from the Nordic seas into the North Atlantic Ocean across the Greenland-Iceland-Scotland Ridge (i.e., Denmark Strait (DS) and Faroe Bank Channel (FBC)) is also a fundamental component of the North Atlantic thermohaline circulation [*Hansen et al.*, 2001, 2004]. The volume flux of the overflows through the Denmark Strait and the Faroe Bank Channel and their sum are shown in Figure 10. Overflow is defined here as water colder than 3.0°C with densities (σ_t) in excess of 27.9 kg m^{-3}. We also compute the flux of water that is colder than 0.3°C over these two major sills, which is shown as a dashed curve. This mode water is thought to account for about two-thirds of the total overflow flux [*Hansen et al.*, 2001], however in our analysis this fraction is about 50%. There is a sustained reduction of about 0.4 Sv in the southward transport of overflow across the Denmark Strait giving a rate of −0.09 Sv decade^{-1} during the last four decades, which is significant at a 90% confidence level using an *F* test. This is in contrast with previous studies, which have no sustained
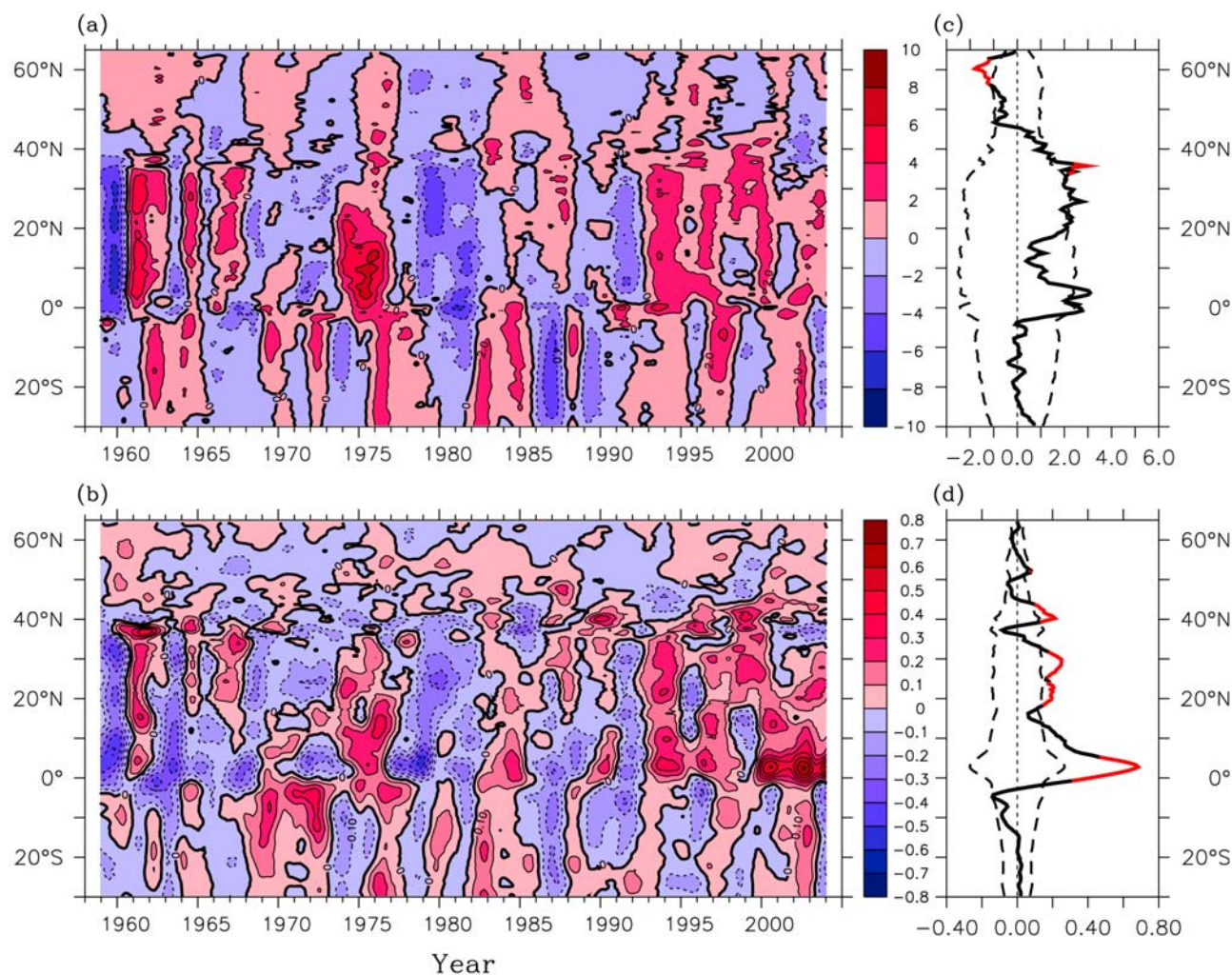
Figure 8. Temporal evolution of anomalous strength of the (a) Atlantic MOC and (b) meridional heat transport for the period 1958–2004. A 47 year linear change in the strength of the (c) Atlantic MOC and (d) meridional heat transport of the Atlantic Ocean as a function of latitude is shown. One standard deviation is shown by a dashed curve and the curve is red when the change exceeds the 95% significant level. Units are Sv for MOC and PW for meridional heat transport.

changes in the overflow rate in the Denmark Strait [*Dickson and Brown*, 1994; *Curry and Mauritzen*, 2005]. By contrast, the transport of the overflow in the Faroe Bank Channel increases slightly, by 0.1 Sv, for the period 1958–2004 at a rate of 0.02 Sv decade^{-1}. However, this slight increase is not significant at a 90% confidence level. The overflow rate in the Faroe Bank Channel was found to have decreased by about 20% from 1950 to 2000 [*Hansen et al.*, 2001]. However, this 20% reduction in overflow strength in the Faroe Bank Channel is not persistent as continuing measurements show that the trend has recently stopped and perhaps has even changed sign [*Curry and Mauritzen*, 2005]. The change in the flux of cold water colder than 0.3°C through FBC is significant at a 90% confidence level. Thus the flux of NADW in the northern North Atlantic Ocean for the period 1958–2004 is also determined by a change of the overflows. Note that the sum of the Faroe Bank Channel overflow (~2.3 Sv) and the Denmark Strait overflow (~3.4 Sv) which accounts for about one-third of the total

NADW flux (~18 Sv), decreases up to 0.3 Sv at an average rate of −0.07 Sv decade^{-1}. This represents a 5% reduction from 1958 to 2004 in the volume flux of the overflows across the Denmark Strait and Faroe Bank Channel sills, which is significant at a 90% confidence level. This trend is similar when applied to a mode water colder than 0.3°C. Thus there is a total reduction of 0.3 Sv in water which has a mean transport of 2.7 Sv. This represents an 11% decrease of southward flux of overflow colder than 0.3°C from 1958 to 2004. This reduction of overflow flux is consistent with the steadily declining salinity in the overflows [*Curry and Mauritzen*, 2005]. Even though the overall southward overflow flux appears to be decreasing during the past four decades, primarily due to a significant decrease in DS, the combined overflow fluxes in both DS and FBC increases in the last ten years of the analysis (1995–2004); consistent with the findings of *Curry and Mauritzen* [2005]. Overall our analysis suggests that the change in the volume flux of the Nordic Seas overflows appears to have decreased slightly
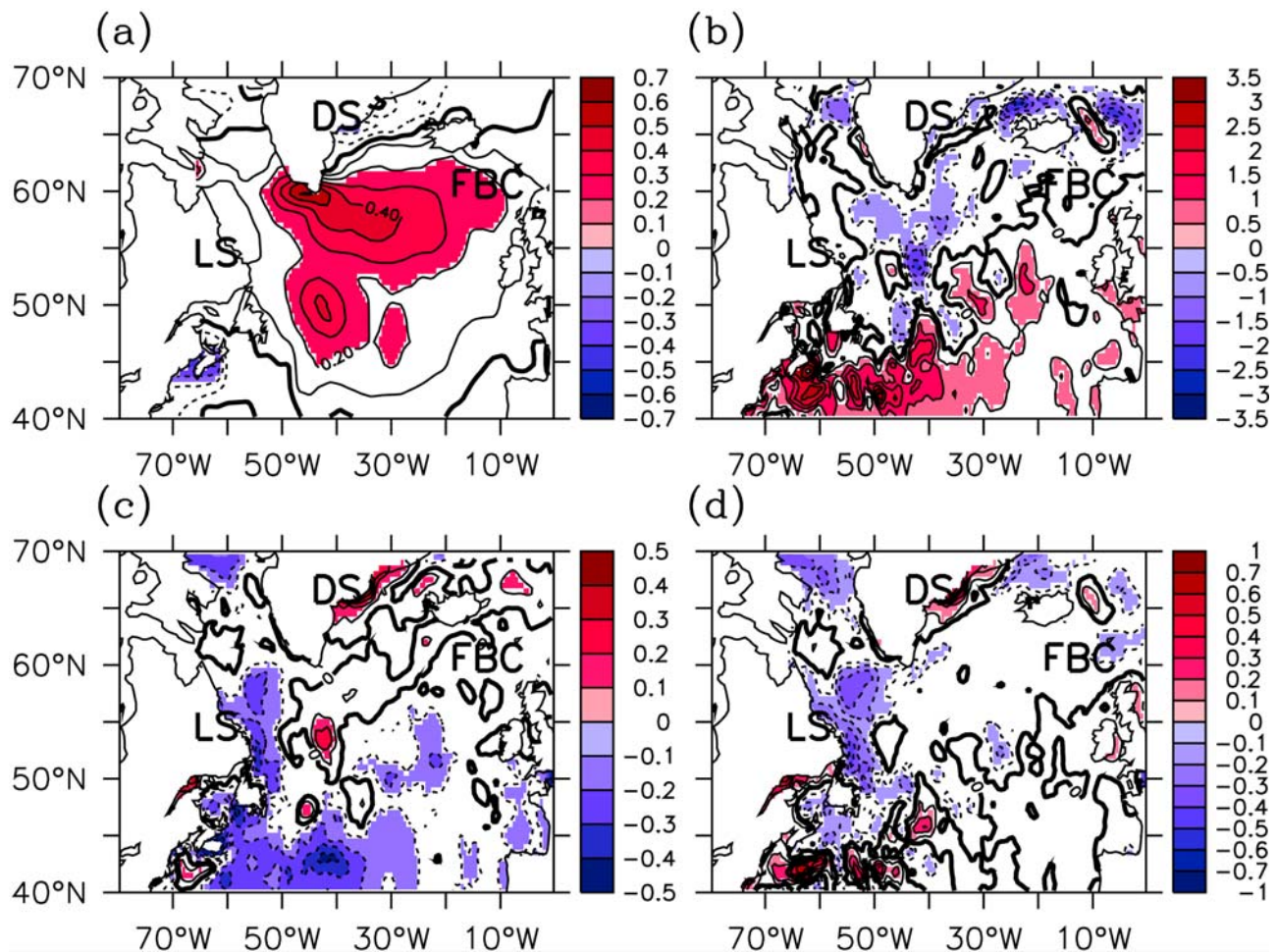
Figure 9. Linear change in (a) zonal wind stress, (b) SST, (c) surface density, and (d) surface salinity of the North Atlantic Ocean for the period 1958–2004. Wind stress τ_x values greater than ±0.2 dynes cm^{-2}, SST values greater than ±0.5°C, density ρ values greater than ±0.1 kg m^{-3}, and salinity values greater than ±0.1 g kg^{-1} are shaded. The Labrador Sea (LS), Denmark Strait (DS), and Faroe Bank Channel (FBC) are marked.

from 1958 to 2004, as summarized in Table 1. Our analysis also suggests that the freshening in the Labrador Sea and slightly decreased overflow together give rise to a slightly weaker MOC in the northern North Atlantic Ocean.

3.5.2. Strengthening in Low to Middle Latitudes

[28] Figure 11 shows the long-term mean winds and the difference of wind stress between two 20 year periods, 1958–1980 and 1981–2001. Between these two periods, the atmospheric circulation strengthens north of 45°N and south of 30°N. As a consequence, there is a considerable convergence of flow due to change in the curl of wind stress between 30°N and 50°N and an enhanced subtropical gyre circulation. The resulting convergence of flow can push water down to deep layers, where it connects with the NADW and moves southward. In addition there is a vertical recirculation in the layer from the surface to 2000 m between 30°N and 50°N (Figure 6c), which is intensified by wind forcing and increases meridional heat transport. In the tropics the change in curl is not as large as at middle latitudes and because the thermocline in the tropics is shallow, enhanced easterlies in both hemispheres produce persistent strong Ekman divergence of flow and strong

upwelling near the equatorial region. This gives rise to a stronger STC that affects the upper layer to a depth of 1000 m. In addition, the enhanced subtropical gyre circulation brings more water north, where it is more efficiently cooled.

[29] What causes the change in atmospheric circulation? One possibility is that the atmospheric circulation pattern over the North Atlantic Ocean shifted northward. The change between the 20 year periods in zonal averaged τ_x as a function of latitude is also shown in Figure 11c and suggests that there is a northward shift in the atmospheric circulation over the North Atlantic Ocean. This northward shift of the atmospheric circulation (highlighted by the difference between black and red curves) results in wind stress anomalies, shown in green in Figure 11c. The meridional shift can be quantitatively estimated as the distance (in degrees) from the location where the zonal average τ_x is zero to the location (very close to 30°N) where the temporal mean zonal average τ_x over 1958–2001 is zero. This is shown in Figure 11d. The resulting shift in atmospheric circulation is 1.6° from 1958 to 2001 at a linear rate of 0.4° per decade. The amplitude change from such a
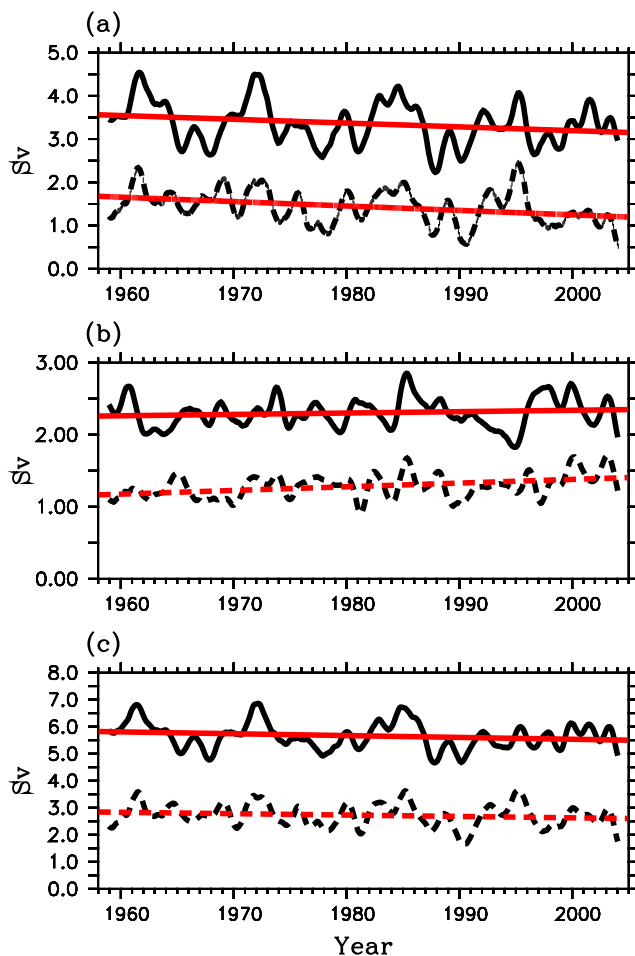
Figure 10. Volume flux of overflow through the (a) DS, (b) FBC, and (c) sum of DS and FBC. The linear trends in the overflow flux are shown as dashed lines. The overflow is defined as the water colder than 3°C with densities σ_t in excess of 27.9 kg m^{-3} (solid curves). Also shown is the flux of water below the 0.3°C isotherm through the DS, FBC, and DS and FBC (dashed curves). Units are Sv.

shift may be important in generating wind stress anomalies, particularly at high latitudes. This interpretation is consistent with the Intergovernmental Panel on Climate Change Fourth Assessment Report (IPCC AR4) for changes in atmospheric circulation. For example, poleward shifts in surface wind stress are found and tend to be accompanied by a consistent poleward shift of the storm track in an ensemble of 21st century climate simulations performed by 15 coupled climate models [*Yin*, 2005]. Therefore, strengthening of MOC in the midlatitude is at least influenced by momentum flux convergences of wind stress due to the northward shift in surface wind stress.

4. Robustness of Surface Forcing Trends

4.1. Surface Wind Stress

[30] Results from SODA show that both momentum forcing in the North Atlantic Ocean and density forcing in the Labrador Sea play important roles in determining MOC variability. Here we address the issue of how sensitive the

results are to the surface forcing used by SODA. First we compare the trends in wind stress from ERA-40 (used by SODA) with trends in wind stress from the National Center for Environmental Prediction-National Center for Atmospheric Research (NCEP-NCAR) Reanalysis 1 (NCEP1 for short), the NCEP-DOE (Department of Energy) Reanalysis 2 (NCEP2 for short), and the Japanese 25 year Reanalysis (JRA-25). A brief summary of the various reanalyses is given in Table 2.

[31] Wind stress from the four reanalyses is plotted in Figure 12 for the three regions we identified as having the largest trends; the northern North Atlantic Ocean (50°W–20°W, 50°N–60°N), the north subtropical Atlantic Ocean (70°W–10°W, 5°N–20°N) and the south tropical Atlantic Ocean (50°W–10°E, 20°S–5°S). All four reanalyses are remarkably consistent in the increasing trend in both the North Atlantic (Figure 12a) and the two tropical regions (Figures 12b and 12c). The combination of increasing trends in both the tropics and in the North Atlantic produce the enhanced convergence leading to the strengthened MOC. The consensus between the reanalyses gives us confidence that the mechanisms described using SODA would be present using other surface momentum forcing fields.

4.2. Precipitation

[32] We also identify freshening of the Labrador Sea and the Nordic seas during the period 1958–2004 as shown in Figure 9d. A similar comparison of surface freshwater forcing was conducted using the CPC Merged Analysis of Precipitation (CMAP) [*Xie and Arkin*, 1997], the NCEP1 and NCEP2 reanalysis precipitation, and GPCP precipitation (Version 2) [*Huffman et al.*, 1997; *Adler et al.*, 2003]. The CMAP precipitation values used in this study are obtained from 5 kinds of satellite estimates (GPI, OPI, SSM/I scattering, SSM/I emission and MSU) as well as blended NCEP/NCAR Reanalysis Precipitation, which covers the period January 1979 to July 2008.

[33] Figure 13 shows the time series of precipitation available from the GPCP, CMAP, NCEP reanalyses as well as salinity (black curve) from SODA averaged in the Labrador and Nordic Seas. The procedure to obtain the time series is the same as to get the time series of zonal wind stress (Figure 12) except that the long-term mean value has been removed for each time series. During the entire period (1958–2004) there is a positive trend in NCEP1 precipitation in the Labrador Sea and Nordic Seas, which favors the generation of surface fresh water in the northern North

Table 1. Volume Flux in Sv of the Overflow Across the DS and the FBC

Location	Definition	Mean[a] (Sv)	Trend[b] (Sv decade^{-1})	Change (1958–2004) (Sv)
DS	T < 3.0°C	+3.4	−0.09	−0.4
	T < 0.3°C	+1.4	−0.10	−0.5
FBC	T < 3.0°C	+2.3	+0.02	+0.1
	T < 0.3°C	+1.3	+0.05	+0.2
DS and FBC	T < 3.0°C	+5.7	−0.07	−0.3
	T < 0.3°C	+2.7	−0.05	−0.3

[a]Southward transport is positive.
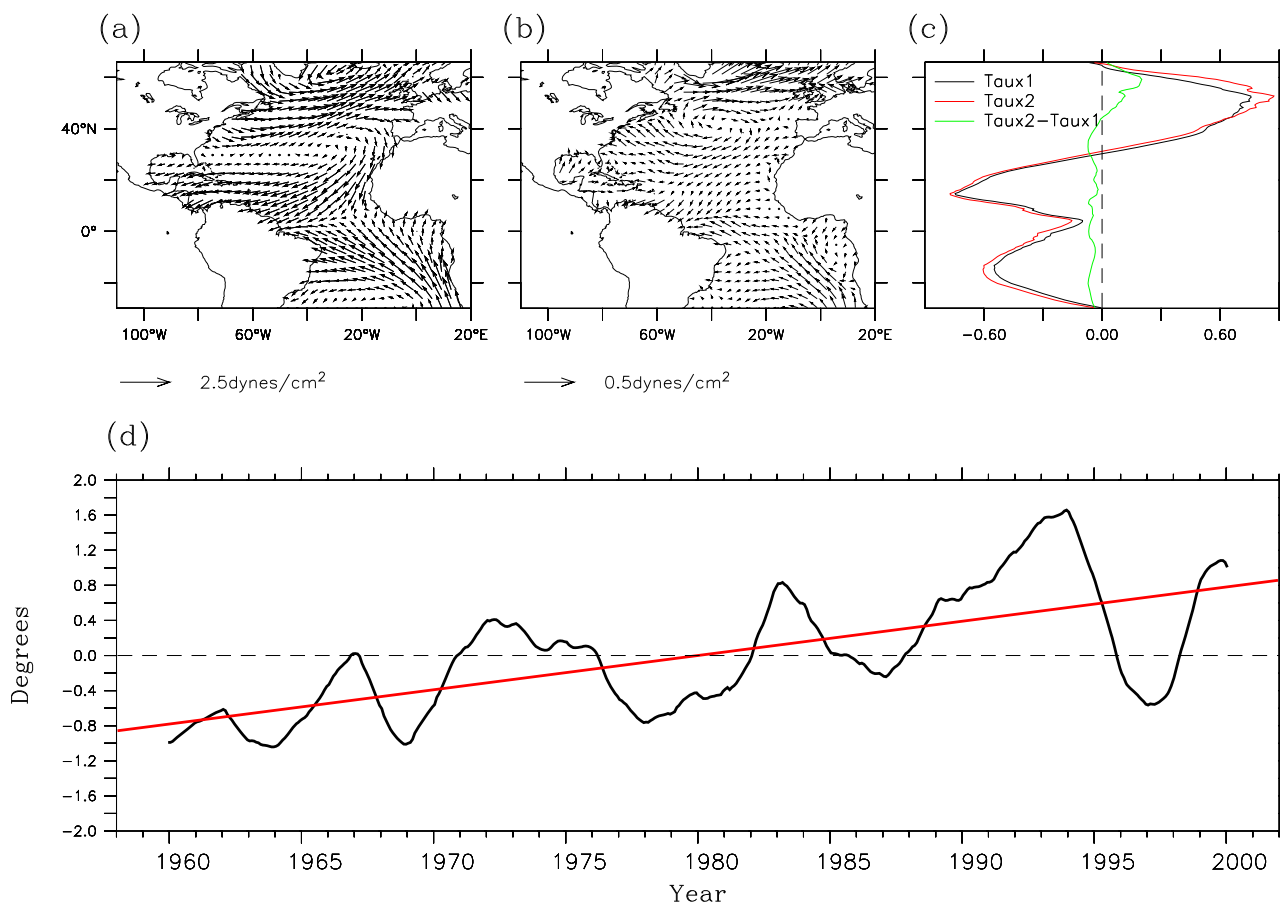[b]Here "+" denotes positive trend of southward flux.

Figure 11. Mean wind stress over the Atlantic Ocean for the (a) period 1958–2001 and (b) difference in the wind stress [(1981–2001)–(1958–1980)]. (c) The difference (Taux2 − Taux1) in zonal averaged zonal wind stress between the period 1981–2001 (Taux2) and 1958–1980 (Taux1) is shown. (d) The implied meridional shift (in degrees) of zonal averaged zonal wind stress is displayed along with its linear trend in red. There is a linear northward shift of $0.39°$ decade^{-1}, so there is a total northward shift of $1.56°$ for the period 1958–2001. The units of wind stress are dynes cm^{-2}.

Atlantic Ocean. This is consistent with a decreasing trend in salinity (black dashed line) from SODA. For the period 1979–2004 when GPCP, CMAP, NCEP2 precipitation values are available, in both the Labrador Sea and the Nordic Seas there is a positive trend in precipitation in NCEP1 and NCEP2, whose sign is opposite to that of GPCP and CMAP. GPCP has a relatively strong negative trend in 1979–2004 in the Nordic Seas. In the Labrador Sea, precipitation increases sharply after 2002. Nevertheless, during 1979–2004 the negative trend in precipitation over the northern North Atlantic Ocean from both GPCP and CMAP implies the generation of saltier water there. This is well represented in salinity change (black curve) in Figure 13. Therefore the trend in salinity obtained from SODA is consistent with the trend (change) of precipitation from GPCP and CMAP, at least after 1979.

[34] As shown in Figure 13, the comparison of the precipitation products does not result in the same clarity of interpretation. There are several reasons why this is the case. First, since SODA assimilates temperature and salinity observations, the ocean surface density is not uniquely determined by the surface fluxes. Second, river runoff undoubtedly plays a role in the variability of surface density, but SODA uses climatological river runoff, and so variability in runoff is not captured. It should be noted that the assimilation of observations may be making up for this deficiency in the model. Last, since SODA uses GPCP precipitation, which starts in 1979, a climatology of GPCP

Table 2. Atmospheric Reanalyses Used

Name	Organization	Period	Resolution[a]	Assimilation
ERA-40	ECMWF	Sep 1957 to Aug 2002	TL159 L60	3DVAR
NCEP-NCAR (Reanalysis 1)	NCEP-NCAR	1948 to present	T62 L28	3DVAR
NCEP-DOE AMIP-II (Reanalysis 2)	NCEP-DOE	1979 to present	T62 L28	3DVAR
JRA-25	JMA-CRIEPI	1979–2004	T106 L40	3DVAR

[a]Here T is triangular truncation, TL is triangular with linear reduced Gaussian grid, and L is vertical layers.
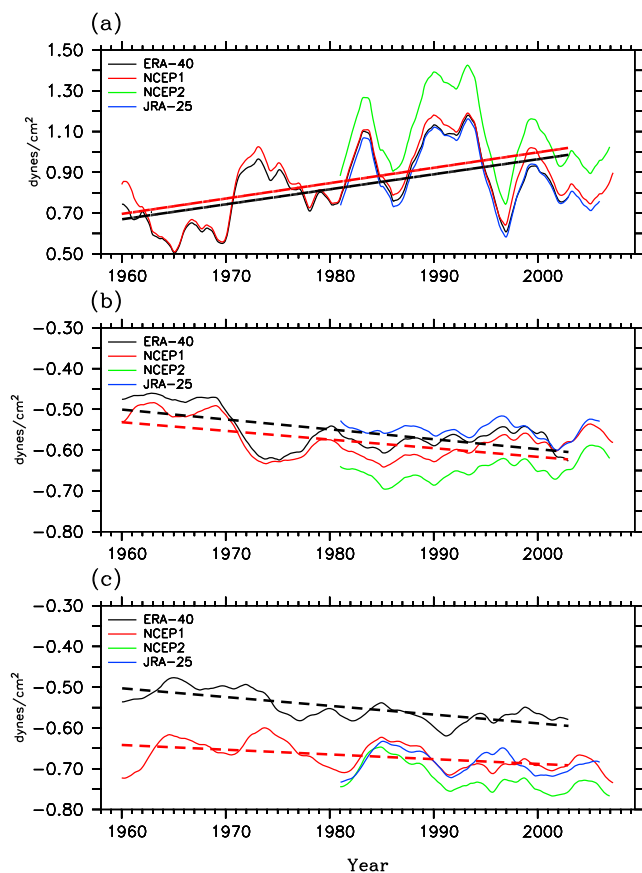
(a)

(b)

(c)

Figure 12. Time series of zonal wind stress (in dynes cm^{-2}) from ERA-40, NCEP1, NCEP2, and JRA-25 averaged over (a) 50°W–20°W, 50°N–60°N; (b) 70°W–10°W, 5°N–20°N; and (c) 50°W–10°E, 20°S–5°S. Trends in area-averaged zonal wind stress from ERA-40 and NCEP1 are denoted by dashed lines in the three regions. The zonal wind stress has been smoothed to show the decadal variability.

precipitation is used, and so variability in precipitation prior to 1979 is not captured by SODA.

5. Conclusions and Discussion

[35] Heat transport in a global ocean analysis is described by exploring its mean, its trend, and its interannual to decadal variability. There are several conclusions that result from this study.

[36] In general the mean heat transport agrees reasonably well with previously reported heat transport estimates from a variety of observational and modeling studies. Of course, the agreement is not expected to be perfect because of the many different periods over which the observations were made. The analysis is also used to calculate the trend of heat transport. The northward heat transport in the Atlantic Ocean is mostly increasing, with increases as large as 25% in some parts of the midlatitude North Atlantic Ocean. This is in distinct contrast with the heat transport estimates of *Bryden et al.* [2005], who analyze data from five hydrographic sections at 25°N and find a decreasing meridional overturning circulation and a decreasing poleward transport of heat. However, recent observational reports

from *Cunningham et al.* [2007] and *Kanzow et al.* [2007] show that a yearlong average MOC at 26.5°N is 18.7 ± 5.6 Sv with variability ranging from 4.4 to 35.3 Sv over the period from 28 March 2004 to 31 March 2005 that the Rapid Climate Change (RAPID) mooring array spans. The range of the MOC estimates includes all five MOC values estimated from the snapshots examined by *Bryden et al.* [2005]. Therefore the long-term decrease inferred from these authors may only be a result of large intraannual variability, rather than a true long-term trend.

[37] Robust interannual to decadal variability of ocean heat transport is found in the global ocean. A simple heat decomposition analysis indicates that it is ocean dynamics (the $V' \overline{T}$ process) that dominates the fluctuation of ocean heat transport in the Oceans. However, at high latitudes in the Pacific and Atlantic Oceans, thermal effects (the $\overline{V} T'$ process) in ocean heat transport become important. Especially in the northern North Atlantic Ocean, fluctuation of temperature is more important than that of varying ocean currents. In the Gulf Stream and its extension region in the Atlantic Ocean and the Kuroshio and Kuroshio extension region in the Pacific Ocean, eddies make an important contribution to ocean heat transport variability, even though
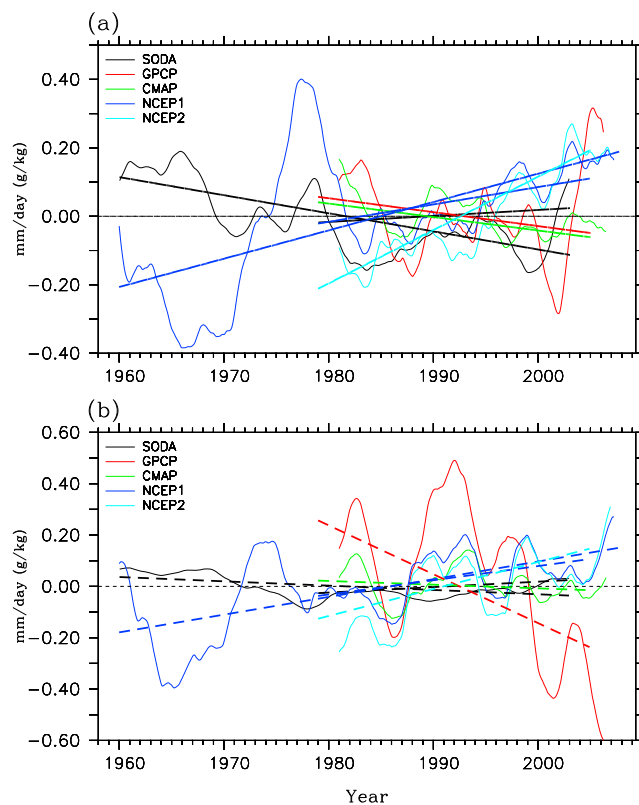
(a)

(b)

Figure 13. Time series of salinity (in g kg^{-1}) from SODA along with precipitation rate (in mm day^{-1}) from GPCP, CMAP, NCEP1, and NCEP2 averaged over (a) 60°W–50°W, 50°N–60°N and (b) 30°W–0°E, 60°N–70°N. The long-term mean of each time series has been removed. Dashed lines denote the trends in area-averaged values in the two regions over the periods 1960–2004 and 1979–2004. The scaling in y coordinate for salinity and precipitation rate is the same.
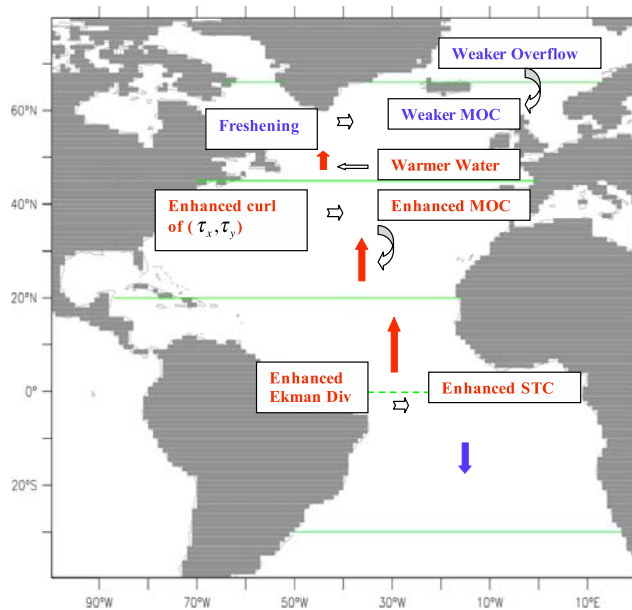
Figure 14. Schematic map of mechanisms of change in the meridional heat transport in the Atlantic Ocean for the period 1958–2004. Red (blue) arrows denote an increase (decrease) of meridional heat transport with respect to its prevalent mean transport.

eddies are not well resolved by the model resolution in SODA. In contrast with the midlatitude Oceans, the change in temperature (the $\overline{U}\,T'$ process) appears to be slightly more important than change in currents (the $U'\,\overline{T}$ process) in the zonal transport of heat in the Southern Ocean.

[38] Mechanisms responsible for the change in ocean heat transport of the Atlantic Ocean during the past four decades are also examined. Ocean heat transport variability is found to be closely associated with changes in the vertical MOC rather than the horizontal gyre circulation. A small increase in meridional heat transport north of 50°N (except at 60°N) seems to be at odds with a slightly weakened high latitude overturning. This oddity reflects the complex processes that control the change of heat transport at high latitude. At high latitude the effect of recent warming in the ocean heat transport grows and becomes comparable to the impact induced by the reduced overturning circulation. The slight weakening of overturning in the northern North Atlantic Ocean results from freshening in the Labrador Sea and the slightly reduced production of Nordic Seas Overflow Water (NSOW) (Figure 9 and Table 1). In the midlatitude ocean, an increased northward heat transport is found which is related to the simultaneous increase of the Atlantic MOC. The increase in the strength of the Atlantic MOC appears to be associated with a northward shift of the atmospheric circulation which produces a strong convergent flow in the ocean, reinforcing the circulation cells to a depth of 3000 m. This interpretation is consistent with the IPCC AR4 Report for changes in atmospheric circulation. It appears that strengthening of MOC at midlatitudes is at least influenced by momentum flux convergences of wind stress due to the northward shift in surface wind stress. A similar air-sea

interaction has been reported by *Giese and Carton* [1999] for the Pacific Ocean.

[39] A reduced northward heat transport in the south tropical Atlantic Ocean and an increased northward heat transport in the north tropical Atlantic Ocean are most likely induced by a strengthened STC. The enhanced STC is primarily driven by stronger Ekman upwelling in the equatorial region, which is closely associated with intensified easterlies. The mechanisms of change in the meridional ocean heat transport in the Atlantic Ocean associated with the Atlantic MOC are summarized in Figure 14. Our analysis suggests that the responsible processes for the variability and the trend of ocean heat transport in the Atlantic Ocean vary in the different regions.

[40] The surface wind stress trends in the SODA analysis are similar to the trends in several other atmospheric reanalyses, giving us confidence that the trends are not an artifact of a particular reanalysis. Our results concerning fresh water flux are consistent with other independent observational studies [*Hansen et al.*, 2001, 2004; *Curry and Mauritzen*, 2005] as well as those derived from CMAP in which numerous satellite observations are involved. However, there is not a consensus regarding trends of surface freshwater forcing between the reanalyses and data sets, and this exists as a primary source of uncertainty in our analysis, and so we have less confidence in identifying trends in density forcing.

References

Adler, R. F., et al. (2003), The version-2 Global Precipitation Climatology Project (GPCP) monthly precipitation analysis (1979–present), *J. Hydrometeorol.*, **4**, 1147–1167, doi:10.1175/1525-7541(2003)004<1147: TVGPCP>2.0.CO;2.

Bennett, A. F. (1978), Poleward heat fluxes in the Southern Hemisphere Oceans, *J. Phys. Oceanogr.*, **8**, 785–798, doi:10.1175/1520-0485(1978) 008<0785:PHFISH>2.0.CO;2.

Boyer, T. P., C. Stephens, J. I. Antonov, M. E. Conkright, R. A. Locarnini, T. D. O'Brien, and H. E. Garcia (2002), *World Ocean Atlas 2001*, vol. 2, *Salinity, NOAA Atlas NESDIS*, vol. 50, NOAA, Silver Spring, Md.

Bryan, K. (1962), Measurements of meridional heat transport by ocean currents, *J. Geophys. Res.*, **67**, 3403–3414, doi:10.1029/JZ067i009p03403.

Bryden, H. L., H. R. Longworth, and S. A. Cunningham (2005), Slowing of the Atlantic meridional overturning circulation at 25°N, *Nature*, **438**, 655–657, doi:10.1038/nature04385.

Carissimo, B. C., A. H. Oort, and T. H. Vonder Haar (1985), Estimating the meridional heat transport in the atmosphere and ocean, *J. Phys. Oceanogr.*, **15**, 82–91, doi:10.1175/1520-0485(1985)015<0082:ETMETI> 2.0.CO;2.

Carton, J. A., and B. S. Giese (2008), A reanalysis of ocean climate using Simple Ocean Data Assimilation (SODA), *Mon. Weather Rev.*, **136**, 2999–3017, doi:10.1175/2007MWR1978.1.

Carton, J. A., G. A. Chepurin, X. Cao, and B. S. Giese (2000), A Simple Ocean Data Assimilation analysis of the global upper ocean 1950–1995, part I: Methodology, *J. Phys. Oceanogr.*, **30**, 294–309, doi:10.1175/ 1520-0485(2000)030<0294:ASODAA>2.0.CO;2.

Cunningham, S. A., et al. (2007), Temporal variability of the Atlantic meridional overturning circulation at 26.5°N, *Science*, **317**, 935–938, doi:10.1126/science.1141304.

Curry, R., and C. Mauritzen (2005), Dilution of the northern North Atlantic Ocean in recent decades, *Science*, **308**, 1772–1774, doi:10.1126/science. 1109477.

Dickson, R. R., and J. Brown (1994), The production of North Atlantic Deep Water: Sources, rates and pathways, *J. Geophys. Res.*, **99**, 12,319–12,341, doi:10.1029/94JC00530.

Fasullo, J. T., and K. E. Trenberth (2008a), The annual cycle of the energy budget. Part I: Global mean and land-ocean exchanges, *J. Clim.*, *21*, 2297–2312, doi:10.1175/2007JCLI1935.1.

Fasullo, J. T., and K. E. Trenberth (2008b), The annual cycle of the energy budget. Part II: Meridional structures and poleward transports, *J. Clim.*, *21*, 2313–2325, doi:10.1175/2007JCLI1936.1.

Fillenbaum, E. R., T. L. Lee, W. E. Johns, and R. Zantopp (1997), Meridional heat transport variability at 26.5°N in the North Atlantic, *J. Phys. Oceanogr.*, *27*, 153–174, doi:10.1175/1520-0485(1997)027<0153:MHTVAN>2.0.CO;2.

Friedrichs, M. A. M., and M. M. Hall (1993), Deep circulation in the tropical North Atlantic, *J. Mar. Res.*, *51*, 697–736, doi:10.1357/0022240933223909.

Ganachaud, A., and C. Wunsch (2000), Improved estimates of global ocean circulation, heat transport and mixing from hydrographic data, *Nature*, *408*, 453–457, doi:10.1038/35044048.

Ganachaud, A., and C. Wunsch (2003), Large-scale ocean heat and freshwater transports during the World Ocean Circulation Experiment, *J. Clim.*, *16*, 696–705, doi:10.1175/1520-0442(2003)016<0696:LSOHAF>2.0.CO;2.

Giese, B. S., and J. A. Carton (1999), Interannual and decadal variability in the tropical and midlatitude Pacific Ocean, *J. Clim.*, *12*, 3402–3418, doi:10.1175/1520-0442(1999)012<3402:IADVIT>2.0.CO;2.

Gouretski, V., and K. P. Koltermann (2007), How much is the ocean really warming?, *Geophys. Res. Lett.*, *34*, L01610, doi:10.1029/2006GL027834.

Hall, M. M., and H. L. Bryden (1982), Direct estimates and mechanisms of ocean heat transport, *Deep Sea Res.*, *29*, 339–359, doi:10.1016/0198-0149(82)90099-1.

Hansen, B., et al. (2001), Decreasing overflow from the Nordic seas into the Atlantic Ocean through the Faroe Bank Channel since 1950, *Nature*, *411*, 927–930, doi:10.1038/35082034.

Hansen, B., et al. (2004), Already the day after tomorrow?, *Science*, *305*, 953–954, doi:10.1126/science.1100085.

Hastenrath, S. (1980), Heat budget of tropical ocean and atmosphere, *J. Phys. Oceanogr.*, *10*, 159–170, doi:10.1175/1520-0485(1980)010<0159:HBOTOA>2.0.CO;2.

Hastenrath, S. (1982), On meridional heat transports in the world ocean, *J. Phys. Oceanogr.*, *12*, 922–927, doi:10.1175/1520-0485(1982)012<0922:OMHTIT>2.0.CO;2.

Holfort, J., and G. Siedler (2001), The meridional oceanic transports of heat and nutrients in the South Atlantic, *J. Phys. Oceanogr.*, *31*, 5–29, doi:10.1175/1520-0485(2001)031<0005:TMOTOH>2.0.CO;2.

Hsiung, J. (1985), Estimates of global oceanic meridional heat transport, *J. Phys. Oceanogr.*, *15*, 1405–1413, doi:10.1175/1520-0485(1985)015<1405:EOGOMH>2.0.CO;2.

Huffman, G. J., et al. (1997), The Global Precipitation Climatology Project (GPCP) combined data set, *Bull. Am. Meteorol. Soc.*, *78*, 5–20, doi:10.1175/1520-0477(1997)078<0005:TGPCPG>2.0.CO;2.

Ivchenko, V. O., N. C. Wells, and D. L. Aleynik (2006), Anomaly of heat content in the northern Atlantic in the last 7 years: Is the ocean warming or cooling?, *Geophys. Res. Lett.*, *33*, L22606, doi:10.1029/2006GL027691.

Jones, P. W. (1999), First- and second-order conservative remapping schemes for grids in spherical coordinates, *Mon. Weather Rev.*, *127*, 2204–2210, doi:10.1175/1520-0493(1999)127<2204:FASOCR>2.0.CO;2.

Kanzow, T., et al. (2007), Observed flow compensation associated with the MOC at 26.5°N in the Atlantic, *Science*, *317*, 938–941, doi:10.1126/science.1141293.

Koltermann, K. P., A. Sokov, V. Terechtchencov, S. Dobroliubov, K. Lorbacher, and A. Sy (1999), Decadal changes in the thermohaline circulation of the North Atlantic, *Deep Sea Res. Part II*, *46*, 109–138, doi:10.1016/S0967-0645(98)00115-5.

Lavin, A., H. L. Bryden, and G. Parilla (1998), Meridional transport and heat flux variations in the subtropical North Atlantic, *Global Atmos. Ocean Syst*, *6*, 231–241.

Macdonald, A. M. (1998), The global ocean circulation: A hydrographic estimate and regional analysis, *Prog. Oceanogr.*, *41*, 281–382.

Molinari, R. L., E. Johns, and J. F. Festa (1990), The annual cycle of meridional heat flux in the Atlantic Ocean at 26.5°N, *J. Phys. Oceanogr.*, *20*, 476–482, doi:10.1175/1520-0485(1990)020<0476:TACOMH>2.0.CO;2.

Newell, R. E., and L. S. Chiu (1981), *Climatic Variations and Variability: Facts and Theories*, edited by A. Berger, pp. 21–61, Reidel, Dordrecht.

Rago, T. A., and H. T. Rossby (1987), Heat transport into the North Atlantic Ocean north of 32°N latitude, *J. Phys. Oceanogr.*, *17*, 854–871, doi:10.1175/1520-0485(1987)017<0854:HTITNA>2.0.CO;2.

Rintoul, S. (1991), South Atlantic interbasin exchange, *J. Geophys. Res.*, *96*, 2675–2692, doi:10.1029/90JC02422.

Robbins, P. E., and J. M. Toole (1997), The dissolved silica budget as a constraint on the meridional overturning circulation of the Indian Ocean, *Deep Sea Res.*, *44*, 879–906, doi:10.1016/S0967-0637(96)00126-4.

Roemmich, D., and C. Wunsch (1985), Two transatlantic sections: Meridional circulation and heat flux in the sub-tropical North Atlantic Ocean, *Deep Sea Res.*, *32*, 619–664, doi:10.1016/0198-0149(85)90070-6.

Schott, F. A., J. P. McCreary Jr., and G. C. Johnson (2004), Shallow overturning circulations of the tropical-subtropical Oceans, in *Earth Climate: The Ocean–Atmosphere Interaction, Geophys. Monogr. Ser.*, vol. 147, edited C. Wang, S.-P. Xie, and J. A. Carton261–304, doi:10.1029/147GM15AGU, Washington, D. C.

Seager, R., Y. Kushnir, P. Chang, N. Naik, J. Miller, and W. Hazeleger (2001), Looking for the role of the ocean in tropical Atlantic decadal climate variability, *J. Clim.*, *14*, 638–655, doi:10.1175/1520-0442(2001)014<0638:LFTROT>2.0.CO;2.

Simmons, A. J., and J. K. Gibson (2002), The ERA-40 project plan, *ERA-40 Proj. Rep. Ser. 1*, 63 pp., Eur. Cent. for Medium-Range Weather Forecasts, Reading, U. K.

Sloyan, B. M., and S. R. Rintoul (2001a), The Southern Ocean limb of the global deep overturning circulation, *J. Phys. Oceanogr.*, *31*, 143–173, doi:10.1175/1520-0485(2001)031<0143:TSOLOT>2.0.CO;2.

Smith, R. D., J. K. Dukowicz, and R. C. Malone (1992), Parallel ocean general circulation modeling, *Physica D*, *60*, 38–61, doi:10.1016/0167-2789(92)90225-C.

Stephens, C., J. I. Antonov, T. P. Boyer, M. E. Conkright, R. A. Locarnini, T. D. O'Brien, and H. E. Garcia (2002), *World Ocean Atlas 2001*, vol. 1, *Temperature, NOAA Atlas NESDIS*, vol. 49, NOAA, Silver Spring, Md.

Sverdrup, H. U., M. W. Johnson, and R. H. Fleming (1942), *The Oceans, Their Physics, Chemistry, and General Biology*, 1087 pp., Prentice-Hall, New York.

Talley, L. D. (1984), Meridional heat transport in the Pacific Ocean, *J. Phys. Oceanogr.*, *14*, 231–241, doi:10.1175/1520-0485(1984)014<0231:MHTITP>2.0.CO;2.

Talley, L. D. (2003), Shallow, intermediate, and deep overturning components of the global heat budget, *J. Phys. Oceanogr.*, *33*, 530–560, doi:10.1175/1520-0485(2003)033<0530:SIADOC>2.0.CO;2.

Trenberth, K. E., and J. M. Caron (2001), Estimates of meridional atmosphere and ocean heat transports, *J. Clim.*, *14*, 3433–3443, doi:10.1175/1520-0442(2001)014<3433:EOMAAO>2.0.CO;2.

Trenberth, K. E., and J. T. Fasullo (2008), An observational estimate of inferred ocean energy divergence, *J. Phys. Oceanogr.*, *38*, 984–999, doi:10.1175/2007JPO3833.1.

Trenberth, K. E., and A. Solomon (1994), The global heat balance: Heat transports in the atmosphere and ocean, *Clim. Dyn.*, *10*, 107–134, doi:10.1007/BF00210625.

Vonder Haar, T. H., and A. H. Oort (1973), New estimate of annual poleward heat transport by Northern Hemisphere Oceans, *J. Phys. Oceanogr.*, *3*, 169–172, doi:10.1175/1520-0485(1973)003<0169:NEOAPE>2.0.CO;2.

Warren, B. A. (1999), Approximating the energy transport across oceanic sections, *J. Geophys. Res.*, *104*, 7915–7919, doi:10.1029/1998JC900089.

Wijffels, S. E., J. M. Toole, H. L. Bryden, R. A. Fine, W. J. Jenkins, and J. L. Bullister (1996), The water masses and circulation at 10°N in the Pacific, *Deep Sea Res.*, *43*, 501–544, doi:10.1016/0967-0637(96)00006-4.

Willis, J. K., J. M. Lyman, G. C. Johnson, and J. Gilson (2007), Correction to "Recent cooling of the upper ocean," *Geophys. Res. Lett.*, *34*, L16601, doi:10.1029/2007GL030323.

Wunsch, C. (2005), The total meridional heat flux and its oceanic and atmospheric partition, *J. Clim.*, *18*, 4374–4380, doi:10.1175/JCLI3539.1.

Xie, P., and P. A. Arkin (1997), Global precipitation: A 17-year monthly analysis based on gauge observations, satellite estimates, and numerical model outputs, *Bull. Am. Meteorol. Soc.*, *78*, 2539–2558, doi:10.1175/1520-0477(1997)078<2539:GPAYMA>2.0.CO;2.

Yin, J. H. (2005), A consistent poleward shift of the storm tracks in simulations of 21st century climate, *Geophys. Res. Lett.*, *32*, L18701, doi:10.1029/2005GL023684.

———————

B. S. Giese, Department of Oceanography, Texas A&M University, MS 3148, College Station, TX 77843-3148, USA.

Y. Zheng, Climate Diagnostics Center, Physical Sciences Division, ESRL, CIRES, NOAA, 325 Broadway, Boulder, CO 80305-3328, USA. (yangxing.zheng@noaa.gov)